Ultrasensitive mid-infrared biosensing in aqueous solutions with graphene plasmon

Chenchen Wu[1,2], Xiangdong Guo[1,2], Yu Duan[1], Wei Lyu[1], Hai Hu[1,2], Debo Hu[1,2], Ke Chen[1,2], Zhipei Sun[3], Teng Gao[1], Xiaoxia Yang[1,2], and Qing Dai[1,2]**

[1]CAS Key Laboratory of Nanophotonic Materials and Devices, CAS Key Laboratory of Standardization and Measurement for Nanotechnology, CAS Center for Excellence in Nanoscience, National Center for Nanoscience and Technology, Beijing 100190, China
[2]Center of Materials Science and Optoelectronics Engineering, University of Chinese Academy of Sciences, Beijing 100049, China
[3]Department of Electronics and Nanoengineering and QTF Centre of Excellence, Department of Applied Physics, Aalto University, Espoo 02150, Finland.
E-mail: daiq@nanoctr.cn, yangxx@nanoctr.cn

Keywords: aqueous solutions, graphene plasmons, surface-enhanced infrared spectroscopy, biosensing

Identifying nanoscale biomolecules in aqueous solutions by Fourier transform infrared spectroscopy (FTIR) provides an in-situ and non-invasive method for exploring the structure, reactions, and transport of biologically active molecules. However, this remains a challenge due to the strong and broad infrared (IR) absorption of water which overwhelms the respective vibrational fingerprints of the biomolecules. In this work, we exploit a tunable IR transparent microfluidic system with graphene plasmon to identify ~2 nm thick protein molecules in physiological conditions. The acquired in situ tunability make it possible to eliminate the IR absorption of water outside the graphene plasmonic hotspots by background subtraction. Most importantly, the ultrahigh confinement of graphene plasmons (confined to ~15 nm) permits the implementation of nanoscale sensitivity. Then, the deuterium effects on monolayer proteins are characterized within an aqueous solution. The tunable graphene plasmon-enhanced FTIR technology provides a novel platform for studying biological processes in an aqueous solution at the nanoscale.

1. Introduction

The length scale of a biomolecule is usually a few nanometers.[1] For instance, proteins are considered the most complex nanoscale molecular machines, and the biomolecular corona interface, the host-pathogen recognition interactions as well as the nanomedicine targeting

effects are at the nanoscale level.[2] Thus, it is important to develop in-situ and non-invasive methods with nanoscale resolutions to understand biological processes in physiological environments.[3] Along these lines, Fourier transform infrared spectroscopy (FTIR) serves as a label-free, non-invasive, and fast method for identifying biomolecules by detecting their molecular vibrational fingerprints.[4] However, achieving FTIR in aqueous solutions with nanoscale sensitivity remains a challenge since the strong and broad infrared (IR) band of water (H_2O) always masks the vibrational fingerprints of the biomolecules, especially in the mid-IR range.[5]

Many efforts have been made to implement the vibrational fingerprints masked by H_2O. For example, other solvents (e.g., D_2O, CCl_4 and CS_2) are used in FTIR measurements since their IR absorption bands are shifted away from the absorption band of H_2O.[4] Another potential route is to shorten the effective IR optical path in an aqueous solution to suppress the interference of H_2O, such as the attenuated total reflectance (ATR).[6] Nevertheless, neither solvent replacement nor ATR can enhance nanoscale sensitivity for the limited FTIR instrumental detection sensitivity. Therefore, the surface-enhanced infrared absorption (SEIRA) technique is developed for in-situ probing nanoscale samples through the evanescent field of the surface plasmons that are directly associated with the inner reflection process.[7] Although the metal plasmon-enhanced FTIR has already achieved high sensitivity, the detection limit is ultimately restricted to monolayer molecules by the relatively poor light confinement of metal in the mid-IR.

The extremely high light confinement of graphene plasmon renders it attractive for SEIRA applications.[8] Interestingly to notice that the sensitivity of graphene plasmon-enhanced FTIR can be enhanced to the sub-nanometer scale, which has been previously applied to identifying molecules in the solid phase and the gas phase.[8a, 9] Graphene has also been employed to increase the infrared absorption of molecules in aqueous solution via the inner reflection process,[10] but the lack of tunability as well as the utilization of bulky ATR instrumentation prevent it from practical use.[11]

In this work, we develop a tunable graphene plasmon-enhanced FTIR technology to identify nanoscale proteins in physiological conditions. Specifically, the H_2O interference outside the graphene plasmon hotspots is eliminated via enforcing an in-situ background subtracting method in the FTIR measurement by gating. Most importantly, the ultrahigh confinement of graphene plasmons (confined to ~15 nm) permits the implementation of nanoscale sensitivity (down to ~2 nm thick proteins). The superior sensitivity in the physiological environment enabled by our approach, in turn, allows the direct monitoring of

the protein hydrogen(H)/deuterium(D) exchange process within an aqueous solution by performing FTIR transmission measurements.

2. The tunable graphene plasmon-enhanced SEIRA in aqueous solutions

The proposed tunable graphene plasmonic aqueous IR (GP-aIR) biosensor is schematically illustrated in Figure 1a. As can be ascertained, it is composed of graphene plasmonic devices and an IR transparent microfluidic system (see details in Methods and Figure S1). It is underlined that the high IR transmittance is the foundation for the implementation of graphene plasmon-enhanced FTIR measurements. To achieve high IR transparency in aqueous FTIR measurements, a 200 μm thick calcium fluoride (CaF_2) crystal is chosen as the top window, whereas a SiO_2/Si substrate supports the graphene plasmonic devices as the bottom window of the microfluidic chamber. More importantly, the height of the microfluidic chamber at the graphene nanoribbon region (100 μm × 200 μm) is designed to be less than 5 μm for ensuring the steady flowing of the solution, as well as a high IR transparency for the FTIR measurements. As a result, the IR absorbance of this microfluidic chamber in the graphene nanoribbon region is less than 0.6 after filling with a protein solution (the blue curve in Figure 1b). We want to state that although CaF_2 crystal (working as a transparent top window) is slightly dissolvable in water, it is found that the GP-aIR biosensor shows high stability and consistent plasmonic response in water for more than 48 hours.

To excite mid-IR plasmons, the graphene on the substrate is patterned to nanoribbon arrays with widths between 50 nm and 100 nm by the electron beam lithography and the oxygen plasma etching (details in Methods and Figure S2). Consequently, a pair of gold electrodes with a titanium adhesion layer are evaporated on graphene as the source and drain contacts, whereas another electrode is evaporated outside graphene to play the role of the gate contact. The sub-nanometer thin electric double layer (EDL) formed on graphene and gold electrodes in the protein solution, works as a dielectric layer of the capacitor so that the graphene Fermi level can be modulated by varying gate voltage based on the parallel plate capacitor theory. On top of that, a 200 nm thick PMMA film as the passivation layer is coated on the source and drain electrodes for preventing the direct interaction of the electrode materials with the aqueous solution and minimizing the current leakage. The extinction spectra are obtained by modulating the gate voltage, i.e., $1\text{-}T_{EF}/T_0$, where T_{EF} is the transmittance measured at a specific graphene Fermi level (EF), whereas T_0 is measured at the graphene charge neutral point (CNP). In addition, there is no graphene plasmon excited at CNP, and we employ T_0 measured at this condition as a background signal for the FTIR measurement. Then, graphene nanoribbons are also doped by gating to excite graphene

plasmons, while the extinction spectrum is measured as $1-T_{EF}/T_0$, which is the plasmonic response of the biosensor system. Thus, the background signal outside the plasmonic hotspot region is eliminated.

The red curve in Figure 1b depicts a typical extinction spectrum as measured with 5 mg/mL protein solution after flowing for 1 hour. It is interesting to notice that two sharp dips at 1545 cm^{-1} (marked with a green line) and 1655 cm^{-1} (marked with a purple line) on the broad graphene plasmonic resonance peak can be detected. This comes from the destructive interference of the graphene plasmon and the molecular vibrations. Therefore, the recorded dip at 1545 cm^{-1} can be identified as the amide II band, which is a typical protein molecular signature. However, the dip at 1655 cm^{-1} is at a region overlapped by the OH-bending mode of the water and the amide I band of the protein. In order to shed light on these outcomes, the region between the wavenumber from 1600 cm^{-1} to 1700 cm^{-1} is magnified and is compared with the extinction spectrum of graphene plasmon in the normal saline (as is divulged in Figure 1c). Without protein, the extinction spectrum of graphene plasmon in the normal saline exhibits the water OH-bending mode at around 1645 cm^{-1} (the grey curve in Figure 1c), while about 10 cm^{-1} shift to the 1655 cm^{-1} for the protein solution can also be recorded (more details can be found in Figure S3).

Surprisingly, the signal strength of the protein exceeds that of water in the extinction spectrum, implying the existence of more protein molecules than water molecules in the plasmon hotspots on the graphene nanoribbons. By carrying out theoretical calculations (see details in Figure S4 and Note 1 in Supporting Information), we found that the density of the protein molecules is enriched by ~3×10^4 times on the graphene nanoribbons compared with that of the protein solution. This result implies the protein adsorption on the graphene surface. Considering our previous works, the physisorption of molecules on graphene is regarded as the driving force.[12] More importantly, a hydrophobic-based graphene surface is more likely to adsorb the protein molecules with hydrophobic groups.[13] Furthermore, the enriched protein molecules on graphene nanoribbons are schematically revealed on the right of Figure 1a. We have to underline that the electromagnetic field distribution is confined around the graphene nanoribbons due to the manifestation of the plasmonic resonances (illustrated as the inset shown in Figure 1c). Therefore, as the protein molecules are adsorbed on the nanoribbon's structures, their IR absorptions are enhanced dramatically by the graphene plasmon. Thus, our tunable graphene plasmon-enhanced FTIR platform discloses superior sensitivity for the identification of proteins even in an aqueous solution.

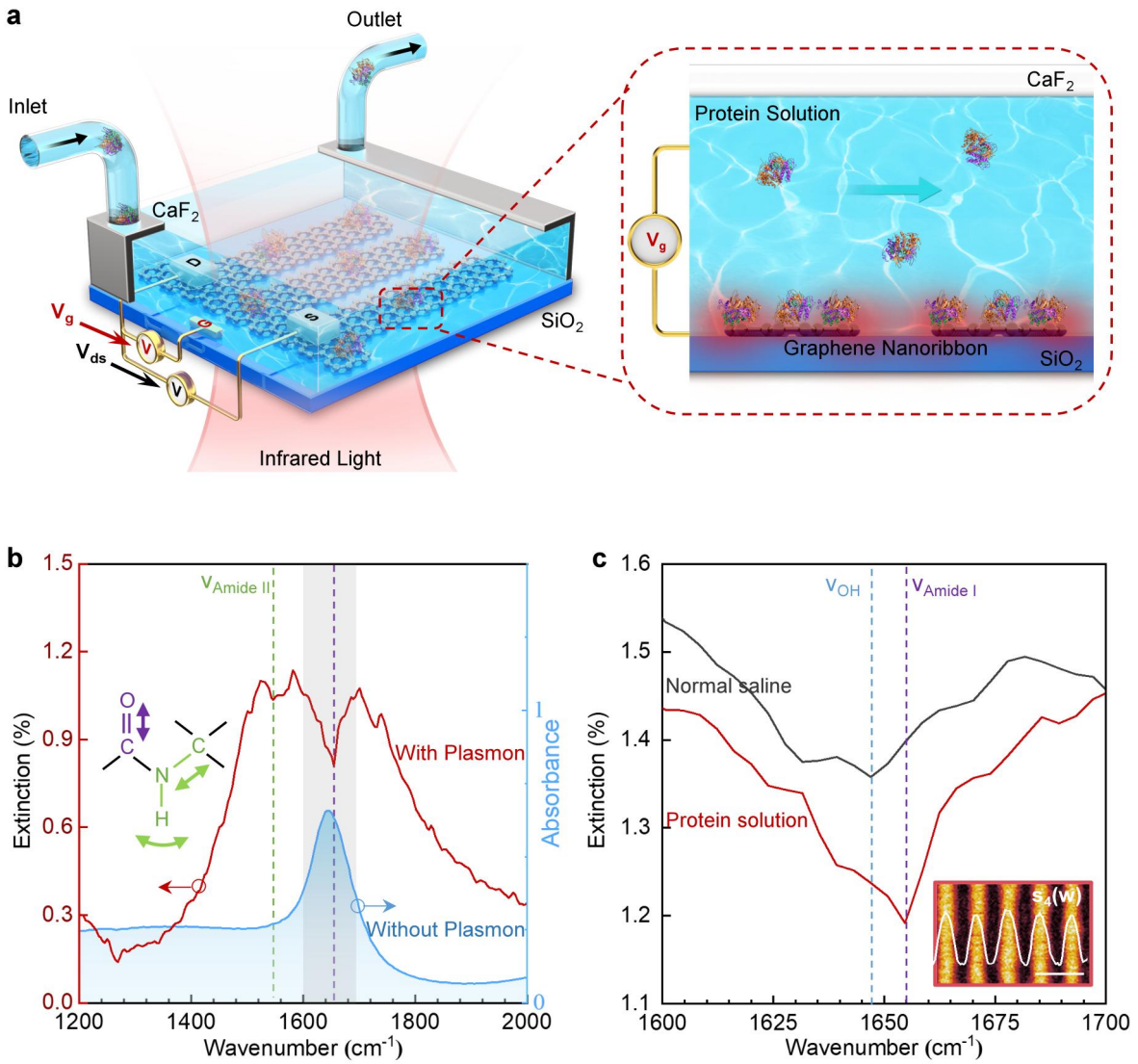

Figure 1. The tunable graphene plasmon-enhanced FTIR platform. (a) Schematic diagram of the GP-aIR biosensor. The microfluidic system is integrated with graphene plasmonic devices and an IR transparent microfluidic system, whereas a 200 μm thick calcium fluoride (CaF_2) crystal is chosen as the top window. Graphene plasmons are excited using an incident infrared light and tuned in-situ by gating. The plasmon resonances are coupled with proteins in the hotspots, thus the fingerprints of proteins are identified. **(b)** Transmission spectrum of protein solution (5 mg/mL) in the microfluidic system with/without graphene plasmon enhancement. **(c)** The magnified mid-IR region (1600-1700 cm^{-1}) for graphene plasmon-enhanced FTIR before (the grey curve) and after (the red curve) protein adsorption in the aqueous solution. E_F=-0.3 eV, graphene nanoribbon width is ~60 nm, the period is ~120 nm; Inset: The near-field optical image of graphene nanoribbon at an IR wavelength of λ=10.526 μm (scale bar is 200 nm).

Additionally, the liquid gate via electric double layer EDL permits the modulation of the graphene plasmons in a wide frequency range. More specifically, a typical transfer characteristic curve of the GP-aIR biosensor after the physisorption–based saturation of the protein molecules in the aqueous solution is highlighted in Figure 2a (blue line). The graphene Fermi energy can be calculated by applying a parallel plate capacitor model. The sub-nanometer thin EDL is formed on both the graphene and gold electrodes in the protein solution, which operates via a liquid gate and has a higher modulation efficiency than the back-gate with the SiO_2 dielectric layer.[14] The estimated liquid-gate capacitance of our GP-aIR biosensor in the protein solution is C_{top}~385 nF/cm^2, whereas the corresponding Fermi energy is depicted by the green curve in Figure 2a (see Note 2 in Supporting Information).

The extinction spectra of the GP-aIR biosensor at different Fermi levels are divulged in Figure 2b. As can be ascertained, the plasmon resonance frequency is dynamically modulated from the value of ~1300 cm^{-1} to 1700 cm^{-1} when the Fermi level is adjusted from ~0.11 eV to 0.25 eV. More importantly, the coupling strength of the protein vibrational mode is enhanced as the detuning of the graphene plasmons and the molecular vibrational modes decrease, which is consistent with the acquired numerical calculation results (the dashed curves in Figure 2b). It is interesting to notice that when the resonance frequency of the graphene plasmons is shifted from ~1200 cm^{-1} to 1560 cm^{-1}, the coupling strength between graphene plasmon and amide II band is enhanced, while the dip at 1545 cm^{-1} is getting even deeper. With the further increase of the Fermi level at the value of 0.25 eV, the dip at the 1545 cm^{-1} becomes shallower, whereas the dip at 1655 cm^{-1}gradually deepens due to the stronger coupling between the amide I band and graphene plasmons. Furthermore, the coupling mechanism between graphene plasmons and molecular vibrational modes can be described as a coupling process between two harmonic oscillators. Although the far-field incident IR light cannot efficiently drive the molecular vibration due to the significant size mismatch, the stronger oscillation properties of graphene plasmon can more efficiently drive the molecular vibrations.[8b, 15] Therefore, it is possible to tune the graphene Fermi energy and realize selective plasmonic response in the mid-IR to identify protein vibrational fingerprints by enforcing different gate voltages.

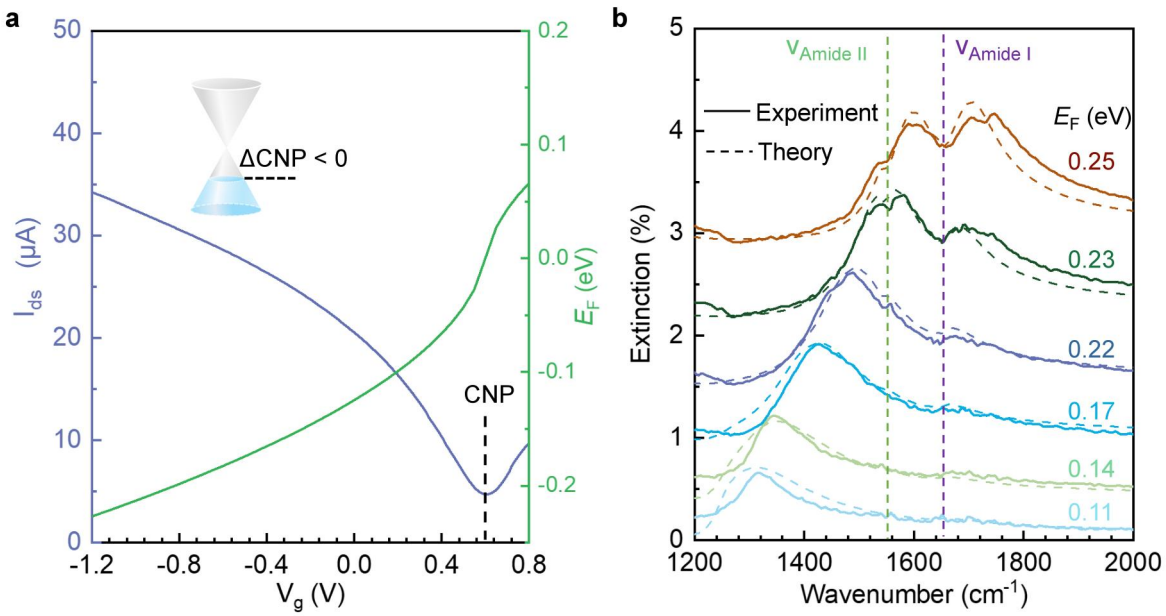

Figure 2. Selective probing of proteins with electrically tunable graphene plasmons. (a) The transfer characteristic curve and the respective Fermi energy of the graphene plasmonic device **(b)** The solid curves are experiment results of graphene plasmon response at different gate voltages; the dashed curves are simulation results of graphene nanoribbon plasmon response are at different Fermi energies. The experimental results are collected after 1 mg/mL protein solution flowing for 2 hours, the graphene nanoribbon width is ~50 nm, and the period is ~100 nm.

3. Protein identification with ultrahigh sensitivity

Here, we investigate the detection limit of the proposed GP-aIR biosensor by monitoring the adsorption process of protein on the graphene nanoribbons. When protein solution is injected into the GP-aIR biosensor, the protein molecules are gradually adsorbed on the graphene nanoribbons and finally reach a saturated state in 20 minutes. The extinction spectra of the GP-aIR biosensor, which are measured at different times during this process, are disclosed in Figure S5. To exhibit the plasmon-enhanced molecular signals more clearly, we extract them from the plasmon resonance peaks in the as-measured extinction spectra, as demonstrated in Figure 3a. At the beginning of injecting the protein solution (0 min), only one broad peak at around 1645 cm^{-1} can be recorded due to the OH-bending mode of the water. As the adsorption time becomes bigger (injecting the protein solution for 7 min, 8 min, 16 min, 20 min), the acquired IR response of the amide II band (~1545 cm^{-1}) appears and constantly enhances as indicated by a green arrow. The IR response near 1645 cm^{-1} is blue shifting to 1655 cm^{-1}, which can be identified as the amide I band of protein (purple arrow).

To further understand the adsorption process, we perform simulations based on the finite-element method (FEM) (see details in Methods). The obtained extinction spectra are in excellent agreement with the respective experimental spectra when considering the adsorbed protein layer with the following thickness values: 0 nm, 2 nm, 4 nm, 6 nm, and 8 nm (Figure 3c). We have also to underline that the thicknesses of the protein layers are consistent with the experimentally measured values. On top of that, we carried out atomic force microscopy (AFM) measurements on the graphene nanoribbons at different adsorption times. The GP-aIR biosensor taken out of the protein solution is washed with deionized water several times and dried in flowing nitrogen. As can be observed from Figure 3b and Figure S6, the height of the graphene nanoribbons increases from ~2 nm to ~8 nm with increasing adsorption time, which verifies that protein molecules are gradually adsorbed on the graphene nanoribbons.

The acquired electrical response can also support the measured results of the proposed GP-aIR biosensor. The protein molecules are negatively charged in our protein solution since its pH value (about 7) is larger than the isoelectric point of the bovine serum albumin (BSA) protein (5.3).[14a] Thus, there are electrons transferred to graphene film after the protein adsorption. In order to exclude the n-doping effect of other ions in the protein solution,[16] normal saline is first injected inside until the CNP of the GP-aIR biosensor stabilizes, and then the protein solution with the same NaCl concentration as normal saline is injected. The transfer characteristics of the GP-aIR biosensor are measured at different times during the protein adsorption process to calculate the induced change of the CNP value (the inset in Figure 3d). As demonstrated in Figure 3d, the protein adsorption shifts the graphene Fermi level toward the Dirac point. It changes fast at the beginning, and then the speed of the change becomes slow and finally reaches saturated adsorption (ΔE_{F}~90 meV). The change law and the time required for the saturated adsorption displayed by the electrical results corroborated the extinction spectra of the GP-aIR biosensor.

These results point out that the GP-aIR biosensor is sensitive to the presence of proteins in an aqueous solution due to the high sensitivity of the graphene plasmons (obvious response for 2 nm protein), as well as to the adsorption of molecules on graphene. In addition, protein solutions with different concentrations are measured, and the outcomes of 100 pg/mL and 100 ng/mL solutions are revealed in Figure S7. After adsorbing protein molecules in the solution for 2 hours, both the amide I and amide II bands can be identified by the GP-aIR biosensor.

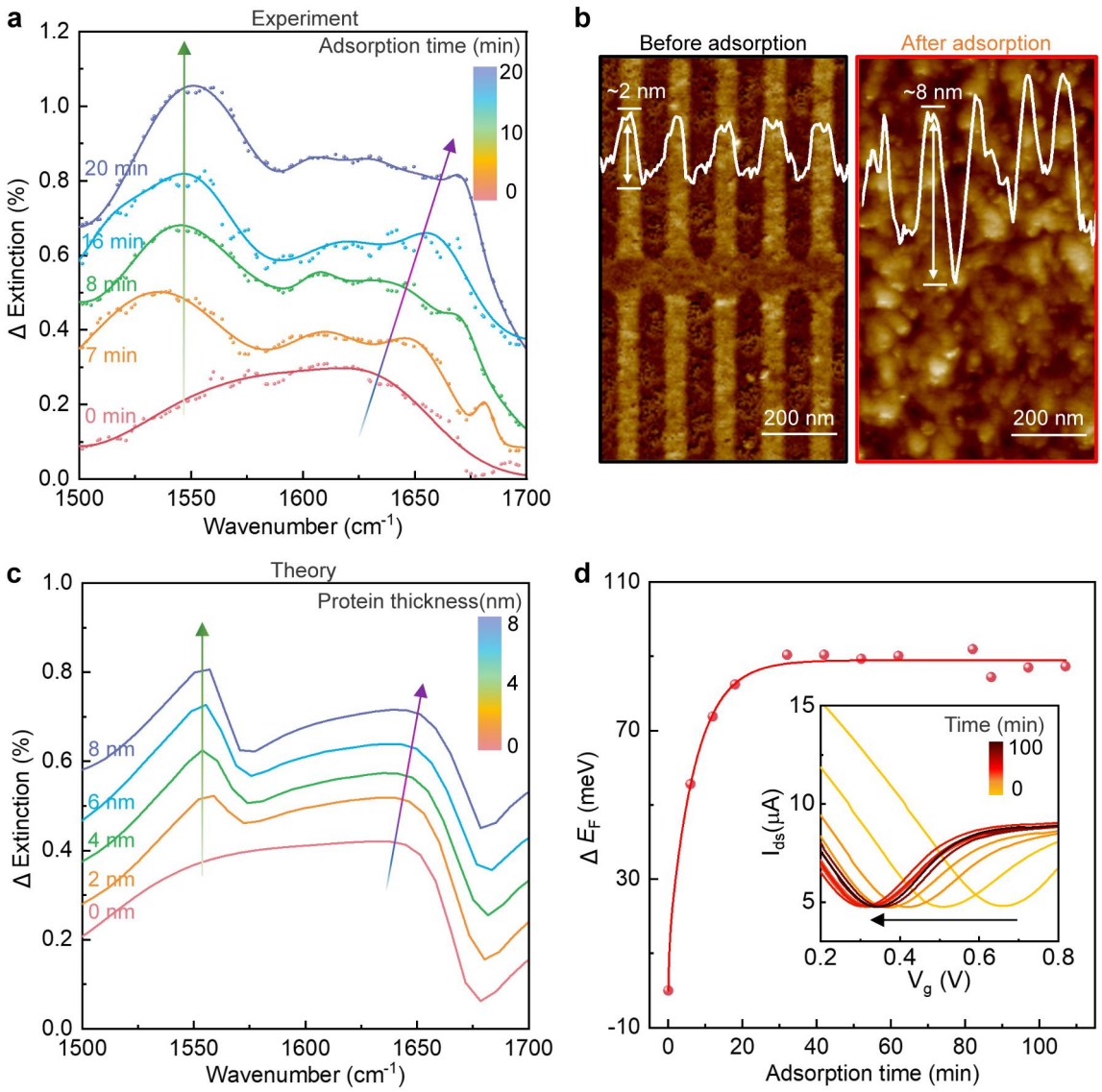

Figure 3. Identification of protein molecules during the adsorption process. (a) Plasmon-enhanced protein IR responses (ΔExtinction) at different adsorption times (0 min, 7 min, 8 min, 16 min, 20 min). The graphene nanoribbon width is ~70 nm, the period is ~140 nm, and the protein solution concentration is 5 mg/mL. **(b)** Morphologies and respective AFM height data of graphene nanoribbons before and after 1 hour of protein adsorption. **(c)** Simulated ΔExtinction of graphene plasmon-enhanced protein IR response with different adsorption thicknesses (0 nm, 2 nm, 4 nm, 6 nm, 8 nm). The parameters of the graphene device are the same as those in (a), and Fermi energy is set as -0.25 eV. **(d)** The Fermi energy changes of the GP-aIR biosensor during protein adsorption in the physiological condition, extracted from the transfer characteristic curves as shown in the inset.

4. Monitoring the H/D exchange process of proteins

H/D exchange is widely used in exploring protein structures and functions for identifying and understanding the complex biological processes and developing pharmaceutical drugs.[17] The exposure of proteins to D_2O induces H/D exchange in disordered regions that lack stable hydrogen bonding. We have to underline that the tightly folded elements are much more protected from the H/D exchange resulting thus in slow isotope exchange.[18] The investigation of the interaction rate and sites of the H/D exchange process between the hydrogens of the protein backbone and its surrounding solvent reflects not only the folded state of the protein and its dynamics but also the intrinsic chemical properties of the underlying amino acid sequence.[17b] Nuclear magnetic resonance spectroscopy (NMR) is currently the most important method to characterize proteins in solution by analyzing the NMR signal of the nuclei of atoms in the protein, but it relies on expensive and complicated equipment and strict sample preparation. A fast and non-invasive method to directly monitor the proton exchange process in an aqueous solution is still missing.

Along these lines, we demonstrate that the tunable graphene plasmon-enhanced FTIR platform can directly monitor the H/D exchange of nanoscale protein molecules within an aqueous solution. Initially, the GP-aIR biosensor is flowing with a protein solution (solvent: H_2O) for 1 hour for reaching saturated adsorption of the protein molecules on the graphene nanoribbons. Subsequently, D_2O is injected into the microfluidic system for half an hour to make sure a complete H/D exchange for the proteins. Then, H_2O and D_2O are alternately injected for several times, while the extinction spectra of graphene plasmon are measured (see Figure S8c). For comparison, the plasmon-enhanced protein responses are extracted and disclosed in Figure 4a. The most obvious change in the acquired spectra is that the peak at 1545 cm^{-1} corresponding to the amide II band disappears and a new peak appears at 1457 cm^{-1} by replacing the H_2O with D_2O, and they recover when reinjecting H_2O. This provides direct evidence for the H/D exchange. According to literature, the peak at 1457 cm^{-1} is assigned to the amide II band of deuterated protein, arising from the coupling of the N-H/D bending and C-N stretching modes (Figure 4b).[19] However, the intensity of the peak at 1457 cm^{-1} is much larger than that at 1545 cm^{-1}, which can be contributed to H-O-D (with bending modes at 1457 cm^{-1}) in D_2O. Due to the hygroscopicity of D_2O, there is also a small amount of H_2O in our D_2O, as manifested by the IR spectrum (see Figure S8a). Additionally, during this H/D exchange process, the amide I band (C=O stretching) of protein at 1655 cm^{-1} has a slight red-shift because hydrogen bonds effects vary on secondary structure in different solvents.

Furthermore, the H/D exchange process on the protein molecular structures in solution by employing different concentrations (17%, 34%, 51%, 68%, 85%) of D_2O is investigated.

Their extinction spectra at each concentration are collected (see Figure S8d), while the plasmonic enhanced signals are extracted and plotted in Figure 4c. Compared with the extinction spectrum in H_2O, the intensities of both the amide I band (around 1655 cm^{-1}) and the amide II band (around 1545 cm^{-1}) decrease by increasing the concentration of D_2O. On top of that, the ratio of H/D exchange is consistent with the ratio of H_2O/D_2O, indicating that the H/D exchange process of nanoscale proteins occurs with high efficiency and reaches a dynamic equilibrium. The reason is that nanoscale proteins have a larger proportion of surface structures exposing to the environment. From this outcome, we can conclude that our approach exhibits high detection sensitivity and can monitor the proton exchange process of nanoscale-based proteins.

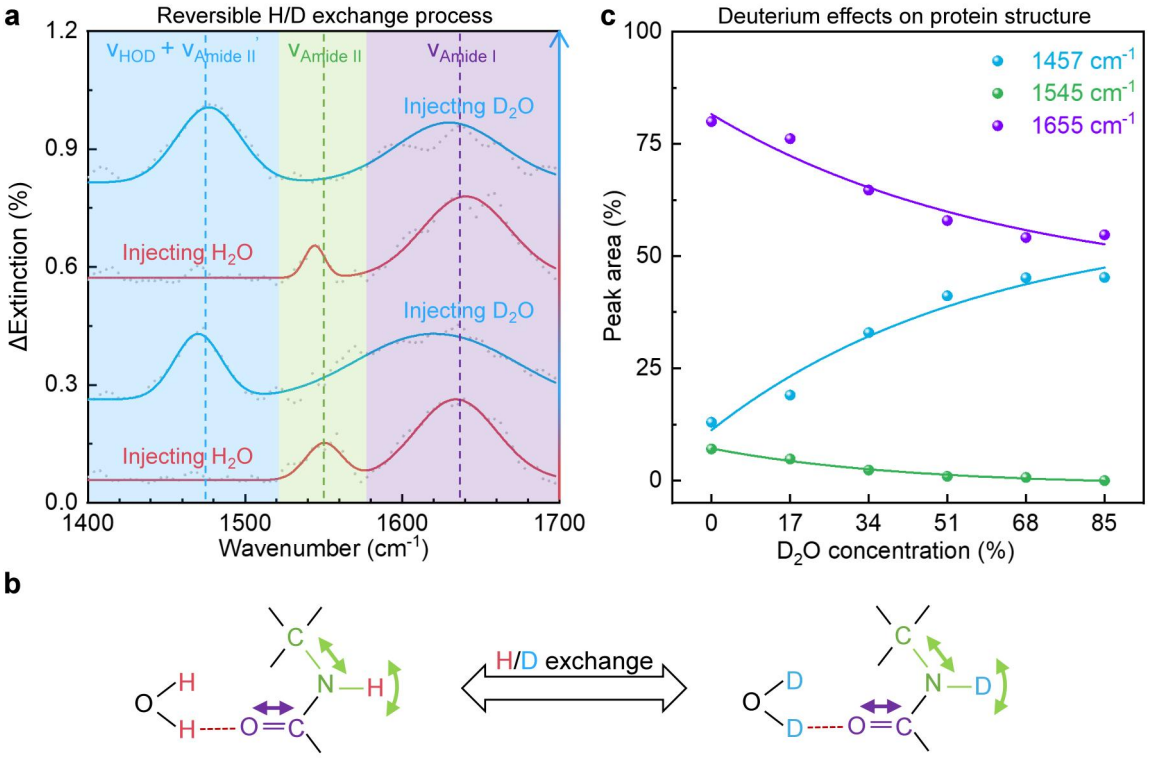

Figure 4. H/D exchange processes monitored by the GP-aIR biosensor. **(a)** In-situ and real-time identification of proteins in H_2O and D_2O which are alternately injected for several times. The protein concentration is 1 mg/mL. The plasmon-enhanced protein responses (ΔExtinction) are extracted from Figure S8c. **(b)** Illustration of D_2O/H_2O induced molecular structure change and hydrogen bond interaction. **(c)** The plasmon-enhanced peak area of ~1457 cm^{-1}, ~1545 cm^{-1}, and ~1655 cm^{-1} are extracted from graphene plasmon-enhanced FTIR at different D_2O concentrations (17%, 34%, 51%, 68%, 85%) in Figure S8d.

5. Conclusion

In conclusion, we adapt graphene plasmons to identify nanoscale protein fingerprints in physiological conditions by employing a tunable graphene plasmon-enhanced FTIR platform. The highly confined optical field and tunability of the graphene plasmons can essentially enhance the light-matter interaction and recede water interference, which pushes the sensitivity down to the value of ~2 nm thick proteins. Meanwhile, we exhibit the dynamic and reversible H/D exchange on the protein molecular structure with the assistance of the GP-aIR biosensor. Interestingly, D_2O is found to affect the nanoscale proteins structures by hydrogen bonds effects on secondary structure and NH/ND exchange on the amide II band. The exciting performance of our approach paves the way for the implementation of an in-situ studying bioprocess within complex physiological conditions with ultrahigh sensitivity, which provides a new strategy for studying the nano-bio interface and opens an inspiring outlook for both nanotoxicology and nano-pharmacology.

6. Methods

Graphene plasmonic IR biosensing in aqueous solutions: The proposed graphene plasmonic devices are composed of connected graphene nanoribbon arrays patterned on a SiO_2/Si substrate by employing electron beam lithography and oxygen plasma etching. Then they are encapsulated with the microfluidic system by utilizing O rings made of nitrile butadiene. The graphene layer is grown on copper foil by chemical vapor deposition method and consequently transferred to a 285 nm SiO_2/500 μm SiO_2 substrate using the wet transfer method. The graphene film is in high quality, as confirmed by the optical image (see Figure S2a), the scanning electron microscope image (see Figure S2b), and the Raman spectra (see Figure S2c). The carrier mobility of the graphene is ~900 $cm^2/(V*s)$, which is extracted from the transfer characteristic curve of the aGP-IR biosensor. Next, the nanoribbon arrays are patterned in graphene by using electron-beam lithography (Vistec 5000+ES, Germany) and then etched with oxygen plasma (SENTECH, Germany). The electrodes (5 nm Ti and 50 nm Au) are patterned and evaporated using electron-beam lithography combined with electron beam evaporation (OHMIKER-50B, Taiwan). Moreover, the in-situ IR microfluidic system is custom-made by Zeptools Co. The thickness of the microfluidic chamber at the graphene nanoribbon region (100 μm * 200 μm) is designed to be less than 5 μm controlled by a gold spacer. In comparison, the thickness of the remaining region is 200 μm which is fabricated by photolithography (SUSS Ma-6, Germany) and deep reactive ion etching (Oxford Plasmalab System 100 ICP 180, England).

Characterization of the graphene plasmon devices: The morphologies and thicknesses of the fabricated graphene nanoribbons are characterized by employing scanning electron microscopy (NOVA Nano SEM 430) and atomic force microscopy (Bruker ICON2-SYS) measurements. As far as the quality of the graphene and defect density of the nanoribbons are concerned, they are measured by Raman spectroscopy (Horiba Jobin Yvon LabRAM HR800) with laser excitation at 514 nm, laser power is 10%, and laser beam spot is ~1 μm. The electrical properties are determined by using a source meter (Keithley 2636B). In addition, FTIR transmission measurements are performed with Thermo Fisher Nicolet iN10 with an IR microscope (10x objective). The aperture is set as 100 μm*200 μm for each measurement, while the resolution is 8 cm^{-1} and scans are 128. The volume required to fill the microfluidic system and permit the steady flow is ~0.1 mL, measured by filling with a syringe pump. The chamber is filled with a protein solution for static measurements, whereas the inlet and outlets are sealed to prevent flow. During the flowing measurements, a constant flow rate of 0.0083 $mL \cdot min^{-1}$ is maintained. The Keithley 2636B source-meter is also employed to tune the top gate voltage.

Near-Field Optical Microscopy Measurements: Near-field imagining is conducted by using a commercially available s-SNOM (Neaspec GmbH), equipped with IR lasers (890-1700 cm^{-1}). The P-polarized IR light from the monochromatic quantum cascade lasers is focused via a parabolic mirror onto both the tip and sample at an angle of 60° to the surface normal. The probes are made initially for metalized atomic force microscope (AFM) with an apex radius of ~20 nm (Nanoworld).

Electromagnetic simulations and theory: The electromagnetic simulations are conducted by using the commercial field solver, COMSOL Multiphysics. The graphene optical response is described via the Drude model. The employed protein solution parameters, including oscillator strength to each FTIR peak, are extracted, and fit the BSA film's measured IR absorbance. The simulation results are calculated by constructing a model utilizing a finite element electromagnetic simulation method. The graphene nanoribbon is modeled as a material with finite thickness and an equivalent relative permittivity distribution that depends on the thickness. The equal relative permittivity ε_g is derived from the surface conductivity σ of the graphene, calculated by the following expression: $\varepsilon_g = 1 + i\sigma/\varepsilon_0\omega t_g$, where ε_0 is the permittivity of the free space, ω is the angular frequency of the incident light, and t_g is the graphene layer thickness. The graphene is modeled as a thin film and treated as the transition

boundary condition with a thickness of just 0.34 nm. At room temperature (T=300 K), the graphene surface conductivity can be approximately calculated from the Drude model:[20]

$$\sigma = \frac{ie^2EF}{\pi\hbar^2(\omega + i/\tau)}$$

e is the electron charge, $\hbar$ is the reduced Planck constant, and EF is the Fermi energy of graphene. The relaxation time $\tau = \mu * EF/ev_F$, where v_F =1×10^6 m/s is the Fermi velocity, and μ ~900 cm^2/(V*s) is the carrier mobility extracted from experimental results.

The protein permittivity is retrieved from the experimental results by adjusting a Lorentzian permittivity:[7c, 8a]

$$\varepsilon_{protein} = \varepsilon_\infty + \sum_{j=1}^{2} \frac{S_k^2}{\omega_j^2 - \omega^2 - i\Gamma_j\omega}$$

The extracted protein permittivity parameters from the experimental protein IR spectrum are: ε_∞=2.08, ω_1=1655 cm^{-1}, ω_2=1545 cm^{-1}, S_1=213 cm^{-1}, S_2=124 cm^{-1}, Γ_1=55.6 cm^{-1}, Γ_1=62 cm^{-1}. The simulation outcomes are in good agreement with the experimental absorption data. In the protein solution, the water IR absorption signal is much stronger than protein molecules. Assuming that proteins are adsorbed on the graphene surface and considering the field contribution of the graphene plasmons, a protein layer with a thickness of 8 nm and a water layer with a thickness of 50 nm is utilized in the model for simplifying the calculation.

The chemicals sampling: The normal saline is 0.9% NaCl solution is prepared by dissolving NaCl (purity larger than 99.5%) in deionized water with a 100 mL volumetric flask. Moreover, the protein solution is prepared by dissolving bovine serum albumin (from KEH, Biotechnology Grade) in normal saline. D_2O is purchased from Macklin with 99.9 atom % D.

Acknowledgements

This work is supported by the National Natural Science Foundation of China (51925203, 52022025, 52102160, 51972074, 11674073, and U2032206), the Key Program of the Bureau of Frontier Sciences and Education, Chinese Academy of Sciences (QYZDB-SSW-SLH021), the Strategic Priority Research Program of the Chinese Academy of Sciences (XDB30000000 and XDB36000000), the Key Research Program of the Chinese Academy of Sciences (ZDBS-SSW-JSC002), Youth Innovation Promotion Association C.A.S., C.A.S. Interdisciplinary

Innovation Team (JCTD-2018-03), and Academy of Finland (314810, 333982, 336144 and 336818), the Academy of Finland Flagship Programme (320167, PREIN), the European Union's Horizon 2020 research and innovation program (820423, S2QUIP; 965124, FEMTOCHIP), the EU H2020-MSCA-RISE-872049 (IPN-Bio), The Business Finland (ALDEL), and ERC (834742).

References

[1] K. A. Dawson, Y. Yan, *Nat. Nanotech.* **2021**, 16, 229.

[2] a) M. P. Monopoli, C. Åberg, A. Salvati, K. A. Dawson, *Nat. Nanotech.* **2012**, 7, 779; b) S. Schöttler, G. Becker, S. Winzen, T. Steinbach, K. Mohr, K. Landfester, V. Mailänder, F. R. Wurm, *Nat. Nanotech.* **2016**, 11, 372; c) P. M. Kelly, C. Åberg, E. Polo, A. O'Connell, J. Cookman, J. Fallon, Ž. Krpetić, K. A. Dawson, *Nat. Nanotech.* **2015**, 10, 472.

[3] a) B. S. Gomes, B. Simões, P. M. Mendes, *Nat. Rev. Chem* **2018**, 2, 0120; b) S. Tenzer, D. Docter, J. Kuharev, A. Musyanovych, V. Fetz, R. Hecht, F. Schlenk, D. Fischer, K. Kiouptsi, C. Reinhardt, K. Landfester, H. Schild, M. Maskos, S. K. Knauer, R. H. Stauber, *Nat. Nanotech.* **2013**, 8, 772; c) F. Chen, G. Wang, J. I. Griffin, B. Brenneman, N. K. Banda, V. M. Holers, D. S. Backos, L. Wu, S. M. Moghimi, D. Simberg, *Nat. Nanotech.* **2017**, 12, 387.

[4] B. H. Stuart, *Infrared spectroscopy: fundamentals and applications*, John Wiley & Sons, **2004**.

[5] a) D. Etezadi, J. B. t. Warner, H. A. Lashuel, H. Altug, *ACS Sens.* **2018**, 3, 1109; b) I. Pupeza, M. Huber, M. Trubetskov, W. Schweinberger, S. A. Hussain, C. Hofer, K. Fritsch, M. Poetzlberger, L. Vamos, E. Fill, T. Amotchkina, K. V. Kepesidis, A. Apolonski, N. Karpowicz, V. Pervak, O. Pronin, F. Fleischmann, A. Azzeer, M. Zigman, F. Krausz, *Nature* **2020**, 577, 52; c) A. G. Brolo, *Nat. Photon.* **2012**, 6, 709.

[6] a) J. D. S. Goulden, D. J. Manning, *Nature* **1964**, 203, 403; b) R. Lu, W.-W. Li, B. Mizaikoff, A. Katzir, Y. Raichlin, G.-P. Sheng, H.-Q. Yu, *Nat. Protoc.* **2016**, 11, 377.

[7] a) R. Adato, H. Altug, *Nat. Commun.* **2013**, 4, 2154; b) O. Limaj, D. Etezadi, N. J. Wittenberg, D. Rodrigo, D. Yoo, S. H. Oh, H. Altug, *Nano Lett.* **2016**, 16, 1502; c) A. John-Herpin, A. Tittl, H. Altug, *ACS Photonics* **2018**, 5, 4117; d) D. Rodrigo, A. Tittl, N. Ait-Bouziad, A. John-Herpin, O. Limaj, C. Kelly, D. Yoo, N. J. Wittenberg, S.-H. Oh, H. A. Lashuel, H. Altug, *Nat. Commun.* **2018**, 9, 2160; e) Y. Jahani, E. R. Arvelo, F. Yesilkoy, K. Koshelev, C. Cianciaruso, M. De Palma, Y. Kivshar, H. Altug, *Nat. Commun.* **2021**, 12, 3246; f) A. John-Herpin, D. Kavungal, L. von Mücke, H. Altug, *Adv. Mater.* **2021**, 33, 2006054; g) C. Wu, A. B. Khanikaev, R. Adato, N. Arju, A. A. Yanik, H. Altug, G. Shvets, *Nat. Mater.* **2012**, 11, 69.

[8] a) O. L. Daniel Rodrigo, Davide Janner,Dordaneh Etezadi, F. Javier García de Abajo,Valerio Pruneri,Hatice Altug, *Science* **2015**, 349, 165; b) X. Yang, Z. Sun, T. Low, H. Hu, X. Guo, F. J. Garcia de Abajo, P. Avouris, Q. Dai, *Adv. Mater.* **2018**, 30, e1704896.

[9] a) I. H. Lee, D. Yoo, P. Avouris, T. Low, S. H. Oh, *Nat. Nanotech.* **2019**; b) H. Hu, X. Yang, F. Zhai, D. Hu, R. Liu, K. Liu, Z. Sun, Q. Dai, *Nat. Commun.* **2016**, 7, 12334; c) X. Yang, F. Zhai, H. Hu, D. Hu, R. Liu, S. Zhang, M. Sun, Z. Sun, J. Chen, Q. Dai, *Adv. Mater.* **2016**, 28, 2931; d) H. Hu, X. Yang, X. Guo, K. Khaliji, S. R. Biswas, F. J. Garcia de Abajo, T. Low, Z. Sun, Q. Dai, *Nat. Commun.* **2019**, 10, 1131.

[10] a) Y. Hu, Á. I. López-Lorente, B. Mizaikoff, *ACS Photonics* **2018**, 5, 2160; b) B. Zheng, X. Yang, J. Li, C.-F. Shi, Z.-L. Wang, X.-H. Xia, *Anal. Chem.* **2018**, 90, 10786.

[11] S.-H. Oh, H. Altug, X. Jin, T. Low, S. J. Koester, A. P. Ivanov, J. B. Edel, P. Avouris, M. S. Strano, *Nat. Commun.* **2021**, 12, 3824.

[12] a) H. Hu, X. Yang, X. Guo, K. Khaliji, S. R. Biswas, F. J. García de Abajo, T. Low, Z. Sun, Q. Dai, *Nat. Commun.* **2019**, 10, 1131; b) K. Khaliji, S. R. Biswas, H. Hu, X. Yang, Q. Dai, S.-H. Oh, P. Avouris, T. Low, *Physical Review Applied* **2020**, 13, 011002.

[13] C. J. Russo, L. A. Passmore, *Nat. Methods* **2014**, 11, 649.

[14] a) Y. Ohno, K. Maehashi, Y. Yamashiro, K. Matsumoto, *Nano Lett.* **2009**, 9, 3318; b) Y.-Q. Bie, J. Horng, Z. Shi, L. Ju, Q. Zhou, A. Zettl, D. Yu, F. Wang, *Nat. Commun.* **2015**, 6, 7593.

[15] F. Neubrech, C. Huck, K. Weber, A. Pucci, H. Giessen, *Chem. Rev.* **2017**, 117, 5110.

[16] a) S. Li, J. Li, Y. Wang, C. Yu, Y. Li, W. Duan, Y. Wang, J. Zhang, *Nat. Electron.* **2021**, 4, 254; b) A. Ahmadian Yazdi, J. Xu, V. Berry, *ACS Nano* **2021**, 15, 6998; c) X. Jia, M. Hu, K. Soundarapandian, X. Yu, Z. Liu, Z. Chen, A. Narita, K. Müllen, F. H. L. Koppens, J. Jiang, K.-J. Tielrooij, M. Bonn, H. I. Wang, *Nano Lett.* **2019**, 19, 9029.

[17] a) J. Atzrodt, V. Derdau, W. J. Kerr, M. Reid, *Angew. Chem. Int. Ed.* **2018**, 57, 1758; b) G. R. Masson, J. E. Burke, N. G. Ahn, G. S. Anand, C. Borchers, S. Brier, G. M. Bou-Assaf, J. R. Engen, S. W. Englander, J. Faber, R. Garlish, P. R. Griffin, M. L. Gross, M. Guttman, Y. Hamuro, A. J. R. Heck, D. Houde, R. E. Iacob, T. J. D. Jørgensen, I. A. Kaltashov, J. P. Klinman, L. Konermann, P. Man, L. Mayne, B. D. Pascal, D. Reichmann, M. Skehel, J. Snijder, T. S. Strutzenberg, E. S. Underbakke, C. Wagner, T. E. Wales, B. T. Walters, D. D. Weis, D. J. Wilson, P. L. Wintrode, Z. Zhang, J. Zheng, D. C. Schriemer, K. D. Rand, *Nat. Methods* **2019**, 16, 595; c) Y. Loh Yong, K. Nagao, J. Hoover Andrew, D. Hesk, R. Rivera Nelo, L. Colletti Steven, W. Davies Ian, W. C. MacMillan David, *Science* **2017**, 358, 1182.

[18] L. Konermann, J. Pan, Y.-H. Liu, *Chem. Soc. Rev* **2011**, 40, 1224.

[19] J. J. Weiss, *Nature* **1964**, 202, 83.

[20] a) M. A. Ordal, L. L. Long, R. J. Bell, S. E. Bell, R. R. Bell, R. W. Alexander, C. A. Ward, *Appl. Opt.* **1983**, 22, 1099; b) D. Rodrigo, A. Tittl, O. Limaj, F. J. G. Abajo, V. Pruneri, H. Altug, *Light Sci. Appl.* **2017**, 6, e16277.